Pattern Recognition in the Ultrasonic Imaging of Reverberant Multilayered Structures

JAFAR SANIIE, MEMBER, IEEE, AND DANIEL T. NAGLE, STUDENT MEMBER, IEEE

Abstract—**Often the existence of reverberations in the ultrasonic pulse-echo imaging of multilayered structure prevents the direct characterization of each layer. The reverberating pattern is governed by the integrity of the layers, and deterioration of these layers can generate complex and unpredictable patterns. Analytical models of classification of reverberant patterns using both normal and oblique angle scanning schemes are presented. The theoretical model has been utilized in the experimental studies of a particular multilayered reverberant environment that exists in the detection of corrosion and/or volatile changes in steam generator tubing used in nuclear power plants. Various reverberant patterns can be recognized that are in close agreement with theoretical predictions.**

INTRODUCTION

THE ULTRASONIC EXAMINATION of multilayered structures using a pulse-echo detection scheme results in multiple reverberant echoes that complicate the characterization of the layers of the target. In the nondestructive evaluation of materials the problem of reverberating patterns arises frequently. In fact, some structures by their very nature are so reverberant that the reverberating echoes comprise the entire signal. Reverberating patterns can occur in the measurements of thin planar defects in metal, in lamination of composite bonds, in gap thickness measurements of metal adhesively bonded systems, oil film measurements, fatigue crack analysis, etc. [1]-[4].

The pulse-echo imaging of reverberant targets consisting of an isolated single layer has been analyzed to some extent in the past [3]-[5]. Reverberations were studied for the case in which the incident sound pulse is of approximately the same or longer duration as the traveling time within the thin layer. It has been found that a moderately accurate thickness measurement be obtained by examining the ratio of the first pronounced peak to the following peak of the backscattered signal [3]. Although this pattern recognition technique is useful for measuring the thickness of a single thin film, it cannot be extended to a structure composed of multiple layers in which each layer causes reverberations.

The mathematical analysis of continuous wave propagation in layered media is known explicitly [6]. However, the use of continuous excitation to characterize a multiple-layered structure requires that the wave must be of a long enough duration to reach a steady-state value. This constraint introduces range ambiguity in the imaging of the target, and the steady-state value represents only the overall characteristics of the multilayered structure. Consequently, the continuous mode of testing lacks the capability of displaying local information, and the characterization of each subsequent layer becomes virtually impossible.

Of particular interest to present research is characterizing the multilayered reverberant environment that exists in the detection of corrosion or volatile changes in the steam-generator tubing system. Steam generators currently in use contain Inconel (steel alloy) tubing, which fits loosely through holes drilled in a carbon steel support structure, as can be seen in Fig. 1(a). Nonprotective magnetite can accumulate on the inner surface of the support plate holes, and if allowed to continue unchecked, will fill the gap and eventually dent or fracture the tube wall. Therefore the periodic inspection of the tube/support structure is needed to assess the degree of corrosion protruding in the water gap and possible deterioration in the tube wall. In examining such structures it is noted that a variety of reverberant patterns can be expected due to the geometry of the layer, or more importantly, the random nature of corrosion growth. These patterns can be recognized and classified for the evaluation of tube/support structures. Through our earlier studies [7], [8], a theoretical model describing the reverberation phenomenon for multilayered structures has been developed that provides critical insight in the characterization of boundaries of multilayered structures.

The tube/support structure is inspected by transmitting an ultrasonic pulse through the tube well, as shown in Fig. 1(b), which results in two dominant sets of reverberating echoes corresponding to the tube wall (tube echoes) and the support plate (support plate echoes). These sets of multiple echoes must be decomposed and separated in order to evaluate the tube/support structure effectively. This paper presents a theoretical model for both normal and oblique angle scanning in conjunction with different processing and pattern-recognition techniques to facilitate the characterization of the tube/support structure in terms of gap size, degree of corrosion growth, and denting.

Manuscript received October 15, 1987; revised February 25, 1988. This work supported by Electric Power Research Institute (EPRI) grants RP2687-3 and RP2673-5.

The authors are with the Department of Electrical and Computer Engineering, Illinois Institute of Technology, Chicago, IL 60616.

IEEE Log Number 8824329.

0885-3010/89/0100-0080$01.00 © 1989 IEEE

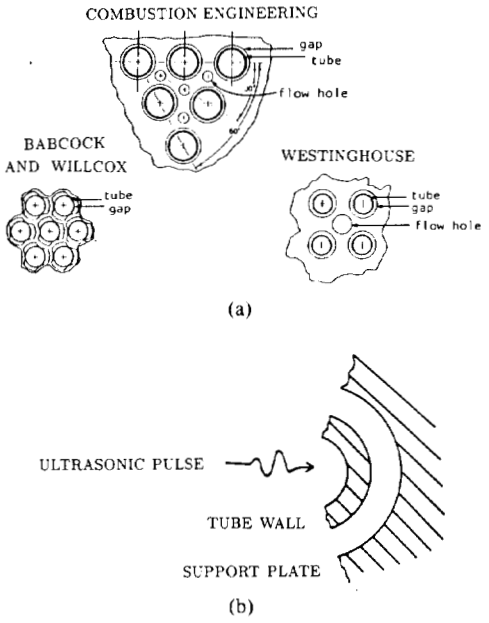

Fig. 1. (a) Typical configuration for tube/support structure. (b) Setup for pulse-echo examination of tube/support structure.

Normal Incident Beam-Echo Classification

For the sake of developing a theoretical base of analyzing the back-scattered echoes from a highly reverberant discrete structure, we will first focus our attention on the simple case of examining a single thin layer. Illustrated in Fig. 2 is an outline of the reverberation process which shows the normal incident beam and the corresponding transmitted and reflected beams as a function of time, where region I, region II, and region III are defined by their density, ρ_i, and the velocity and sound in that media, denoted by v_i. These two quantities define the acoustic impedance, Z_i, of a given region i:

$$Z_i = \frac{1}{\rho_i v_i}. \tag{1}$$

The incident ultrasonic beam impinging the thin layer is partially reflected and transmitted at each boundary as shown in Fig. 2. Using the characteristic impedances, the reflection and transmission coefficients of each boundary can be calculated using

$$\alpha_{ij} = \frac{Z_i - Z_j}{Z_i + Z_j}; \ \beta_{ij} = \frac{2Z_i}{Z_i + Z_j} \tag{2}$$

where α_{ij} and β_{ij} are the reflection and transmission coefficients of adjacent regions i and j, respectively.

The successive reflections and transmissions within a single layer result in multiple received echoes, which can be modeled as

$$r(t) = \alpha_{12}u(t) + \sum_{k=1}^{\infty} a_k u(t - 2kT_2) \tag{3}$$

where

$$a_k = \beta_{12}\beta_{21}\alpha_{23}^{k}\alpha_{21}^{k-1} \tag{4}$$

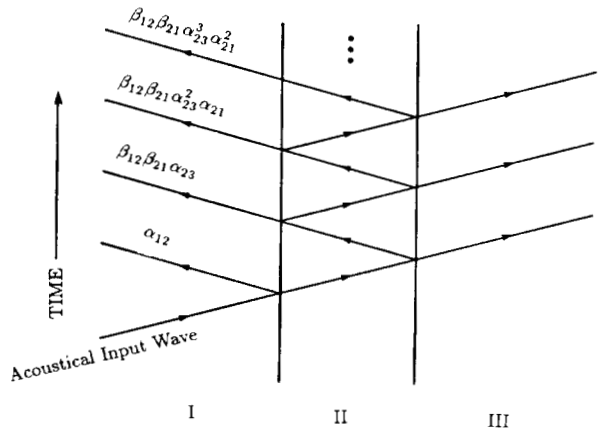

Fig. 2. Reverberation path in single thin layer.

$r(t)$ is the received signal, T_i is the time it takes the echo to travel the ith region, and $u(t)$ is the impulse response of the measuring system. The received signal can be thought of as a set of multiple echoes spaced evenly apart in time, separated by a time $2T_2$. The effect of grain noise and system noise are considered negligible in this derivation and are not included in the preceding equation.

An example of the reverberant pattern resulting from the examination of a thin steel plate is shown in Fig. 3(a). From the measured signal, the thickness of the plate can be determined. The time between echoes is $2T_2$, and this can be used to calculate the thickness of region i, d_i, since

$$d_i = v_i T_i \tag{5}$$

where v_i is the velocity of sound (longitudinal) in the ith region. In addition, the amplitude of sequential echoes decreases by a factor of $\alpha_{23}\alpha_{21}$. This phenomenon, for the case where $\alpha_{23} = \alpha_{21} = \alpha$, is demonstrated for different reflection coefficients α in Fig. 3(b). The least reverberant case is shown in graph I, where most of the energy arrives within the first few echoes. This is due to the low impedance of the thin layer, which allows much energy to escape within the initial reverberations. However, as the thin layer becomes more mismatched with its surroundings, as shown progressively in graphs II–IV, later echoes increase in energy, resulting in prolonged reverberations. Increasing in acoustical mismatch at the interface of the layer makes the signal more reverberant since less energy is allowed to leak out of the layer at each reverberation. The Inconel tube of the tube/support structure can be characterized by the highly reverberant case shown in graph IV, where a drop of 20 dB can be expected from the first reverberation in comparison to the first received echo. Generally, highly reverberant layers let very little energy penetrate and therefore make imaging through the layer more difficult. The envelopes of reverberant echoes contain information that can lead to estimates of α_{ij} and β_{ij} and result in estimates of the acoustical impedance of the layer, Z_j, provided that the attenuation of the layer is negligible or known.

With multilayered structures, the recognition of rever-

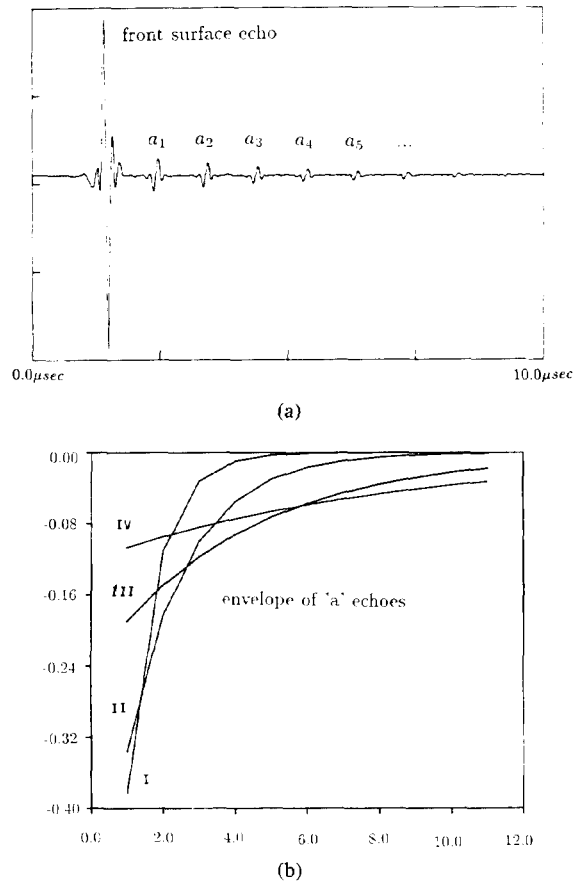

Fig. 3. (a) Back-scattered signal from A-scan of thin steel layer. (b) Envelope of reverberation echoes from thin layer for different values of α: I) $\alpha = 0.54$; II) $\alpha = 0.74$; III) $\alpha = 0.88$; and IV) $\alpha = 0.94$.

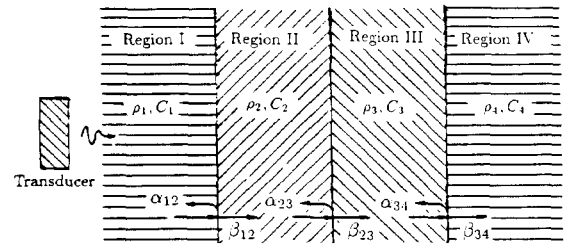

Fig. 4. Multilayered structure consisting of four different regions.

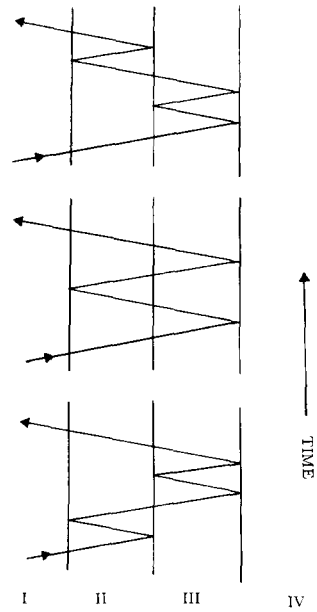

Fig. 5. Variations of wave paths with equivalent traveling time for case where $k = 2$ and $l = 2$.

berant patterns is more complex due to multiple interfering echoes produced at each interface. The tube/support structure can be represented by a model shown in Fig. 4, where region I is inside the tube, region II is the Inconel tube wall, region III is the water gap, and region IV is the steel support plate. In the pulse-echo examination of the tube/support structure, the received signal is comprised of multiple echoes detected after traveling k times in region II and l times in region III:

$$r(t) = \sum_{k=0}^{\infty} \sum_{l=0}^{\infty} \gamma_{kl} u(t - 2kT_2 - 2lT_3) \qquad (6)$$

the term γ_{kl} is the received echo amplitude related to the reflection coefficient, α_{ij}, or the transmission coefficient, β_{ij} (note: i and j indicate which regions constitute the interface). The term γ_{kl} can not be expressed explicitly in terms of α_{ij}, l, and k, since there are many echoes of different intensities and paths traversed that have equivalent travel times. These echoes are then summed together to form a composite amplitude, γ_{kl}. A simple example of this for the case where $k = 2$ and $l = 2$ is shown in Fig. 5, in which there are three unique paths that comprise γ_{22}. For large values of k and l, the number of paths will increase tremendously.

Through extensive experimentation and computer simulation, an appropriate identification and classification technique was developed that allowed characterization of the layered structure represented by detected echoes of significant intensities [8]. As a result of classification the generalized model for the received echoes given in (6) can be presented differently:

$$\begin{aligned} r(t) = {} & \alpha_{12} u(t) + \sum_{k=1}^{\infty} a_k u(t - 2kT_2) \\ & + \sum_{k=1}^{\infty} b_k u(t - 2T_3 - 2kT_2) \\ & + \sum_{k=1}^{\infty} c_k u(t - 4T_3 - 2kT_2) \\ & + \sum_{k=1}^{\infty} d_k u(t - 6T_3 - 2kT_2) + \cdots \end{aligned} \qquad (7)$$

where a_k is the amplitude of the class "a" echoes, which reverberate in region II only; b_k is the amplitude of the class "b" echoes, which reverberate continually in region II and once in region III; c_k is the amplitude of the class "c" echoes, which reverberate continually in region II and twice in region III; d_k is the amplitude of the "d" echoes, which reverberate continually in region II and three times in region III; etc.

The amplitude of these classes of echoes are given [8] as

$$a_k = \left(\frac{\beta_{12}\beta_{21}}{\alpha_{21}}\right)A_0^k; \qquad \text{for } k \geq 1 \tag{8}$$

$$b_k = k\left(\frac{\beta_{12}\beta_{21}}{\alpha_{21}}\right)A_1A_0^{k-1}; \qquad \text{for } k \geq 1 \tag{9}$$

$$c_1 = \frac{\beta_{12}\beta_{21}}{\alpha_{21}}A_2 \tag{10}$$

$$c_k = \left(\frac{\beta_{12}\beta_{21}}{\alpha_{21}}\right)k\left[A_2A_0^{k-1} + \frac{k-1}{2}A_1^2A_0^{k-2}\right]; \quad \text{for } k > 1 \tag{11}$$

$$d_1 = \left(\frac{\beta_{12}\beta_{21}}{\alpha_{21}}\right)A_3 \tag{12}$$

$$d_2 = \left(\frac{\beta_{12}\beta_{21}}{\alpha_{21}}\right)[A_3A_0 + A_2A_1] \tag{13}$$

$$d_k = \left(\frac{\beta_{12}\beta_{21}}{\alpha_{21}}\right)\left[A_3A_0^{k-1} + (k-1)A_2A_1A_0^{k-2} + \frac{(k-1)(k-2)}{6}A_1^3A_0^{k-3}\right]; \qquad \text{for } k > 2 \tag{14}$$

where

$$A_n = \beta_{23}\beta_{32}\alpha_{34}^n\alpha_{32}^{n-1}\alpha_{21}. \tag{15}$$

One of the major advantages of wave classification is that class "b" echoes increase while class "a" echoes decrease. This increase is true for several reverberations and depends solely on the characteristics of region III (or the first thin layer). The effect of region IV (support plate) changes the class "b" linearly, as can be seen in (9). As the impedance of region IV increases, b_n increases, which is a highly desirable situation for detection.

The evaluation of the b_k in terms of k and regions I, II, III, and IV is more involved than in the previous discussion of a_k for the analysis of a single layer. However, insight to the behavior of b_k can be found by examining the maximum of "b" echoes in terms of the reverberation number k:

$$\frac{db_k}{dk} = 0. \tag{16}$$

Hence the solution for k can be determined as

$$k = \frac{-1}{\log \alpha_{21}\alpha_{23}} \tag{17}$$

where k is an integer. The maximum value of b_k varies according to the characteristic impedance of region II relative to regions I and III. The reverberation is prolonged as the impedance of the thin layer increases. On the other hand, for a lower impedance of the thin layer, the strongest "b" echoes are the first few.

Envelopes of class "b" echoes for various characteristic impedances of regions I–IV are shown in Figs. 6(a)–(d). Figs. 6(a)–(d) shows instances of severe-to-mild reverberation in region II. In each figure, graphs I–IV represent insignificant-to-significant acoustical mismatch between regions III and IV, where α_{34} takes on the following values: I) 0.25; II) 0.54; III) 0.74; and IV) 0.93. Fig. 6(a) closely resembles the class "b" echoes of the tube/support structure for various reflection coefficients of the support plate. This is beneficial in determining how deterioration of the support plate will affect the integrity of the signal. Furthermore, these graphical results are very useful in interpreting of the received signal, which leads to determining the best region in time for class "b" echo evaluation. As shown in Fig. 7 (this figure exhibits characteristics very similar to that of the tube/support structure), comparison of the envelopes of the "a" and "b" echoes reveals that the best region for observing "b" echoes is near the eighth reverberation, b_8. A simulated back-scattered signal (A-scan) of the tube/support structure, where the water gap delay is smaller than the reverberation time in the tube wall, can be seen in Fig. 8. This plot gives clear indication of the exact position of both the "a" and "b" echoes. The tube thickness (region II) and gap size (region III) can also be determined from this figure, where the tube thickness corresponds to the delay between the peaks of the echoes within each class, and the gap distance is given by the time delay between the "a" and "b" echoes. Similar discussions hold for class "c," "d," etc. echoes, but their amplitudes are much smaller than class "a" and "b" echoes. In experimental data, detection of these echoes becomes very difficult. Furthermore, no additional information will be gained by their evaluation.

Using a transducer with a center frequency of 20 MHz and a 10-MHz bandwidth, experimental results (shown in Fig. 9) confirm theoretical model predictions. Fig. 9(a) shows the ultrasonic examination of a planar multilayered (consisting of four regions) structure in which the reverberating thin layer is aluminum. Class "a," "b," "c," and "d" echoes exist for several reverberations. As expected, the "a" echoes decrease with time, and it is apparent that the intensity of "b" echoes increases for a few reverberations, which coincides with theoretical findings of the model.

Fig. 9(b) displays the back-scattered signal from an Inconel tube/support structure, which is more reverberant than aluminum. The "a" and "b" echoes are clearly visible, yet are not as pronounced as in the upper trace, and the presence of "c"and "d" echoes is negligible. Thus the previous model can be simplified somewhat by focusing on the two dominant classes of echoes, to give

$$r(t) = \alpha_{12}u(t) + \sum_{k=1}^{\infty} a_k u(t - 2kT_2) + \sum_{k=1}^{\infty} b_k u(t - 2T_3 - 2kT_2) + n(t) \tag{18}$$

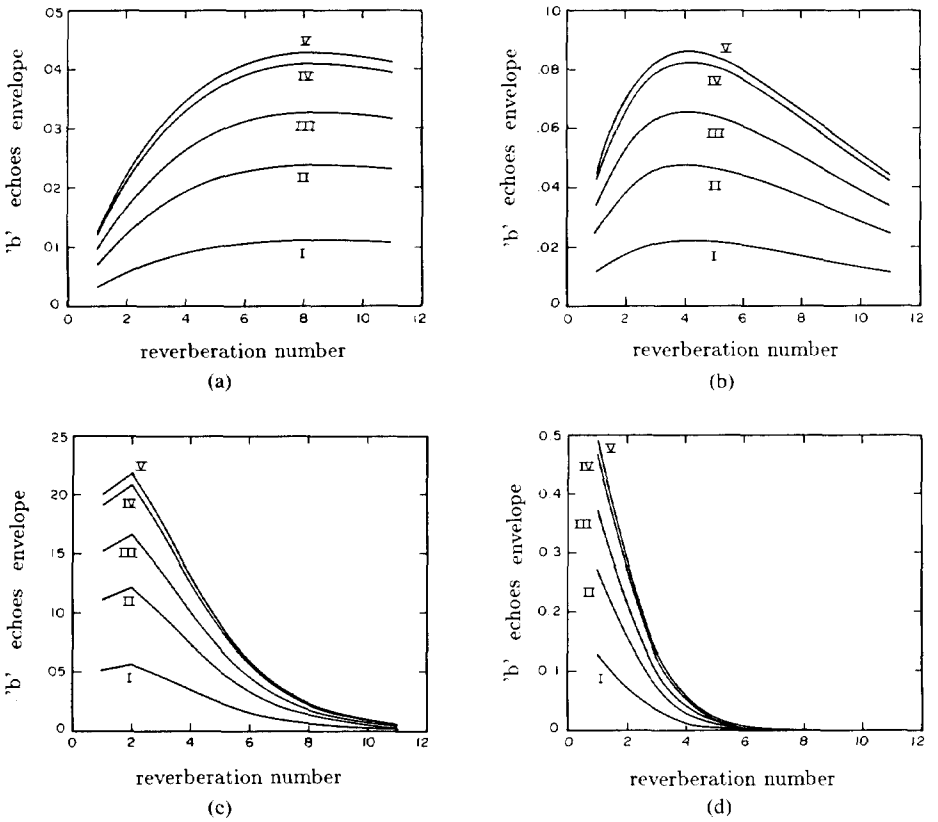

Fig. 6. Envelopes of "b" echoes for various values of α_{34}: I) $\alpha_{34} = 0.25$; II) $\alpha_{34} = 0.54$; III) $\alpha_{34} = 0.74$; IV) $\alpha_{34} = 0.93$; and V) $\alpha_{34} = 0.97$. a) $\alpha = 0.94$. b) $\alpha = 0.88$. c) $\alpha = 0.74$. d) $\alpha = 0.54$. ($\alpha = \alpha_{12} = \alpha_{32}$).

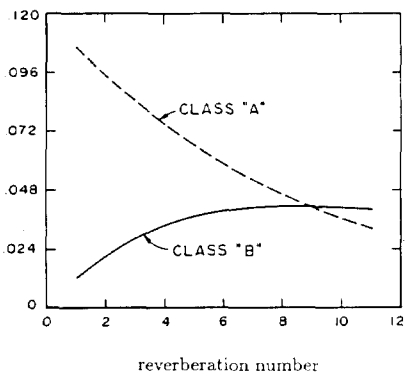

Fig. 7. Comparison of envelope of class "a" echoes (dashed line) with envelope of class "b" echoes (solid line).

where $n(t)$ represents the error, which includes all other low-intensity reverberant echoes not considered and noise introduced by the measuring system. Furthermore, it should be noted that variations in the gap size (region III) can situate the "a" and "b" echoes such that they become close enough to interfere with each other. Also, poor reflective surfaces (i.e., support plate) will cause deterioration in the signal in which the class "b" echoes are severely affected. Thus separation or decomposition would be advantageous in characterizing the tube and support-plate echoes. One method of decomposition involves oblique angle scanning, discussed next, which automatically rejects the interfering tube echoes and thus improves the visibility of the lower-intensity "b" echoes.

Oblique Angle Scanning

Oblique angle scanning (OAS) provides the automatic rejection of "a" echoes (tube echoes) while still preserving the information-bearing "b" echoes (support-plate echoes) in the back-scattered signal [9]. In general, as the scanning angle varies, the degree of refraction and reflection and energy transfer that occurs at each interface changes dramatically and complicates the evaluation of detected multiple echoes. Thus, for this technique to be most effective, the choice of the oblique angle must satisfy the optimality criterion, which means the scanning angle must be chosen to reject a sufficient amount of "a" echoes and maximize the energy of "b" echoes in the received signal. Besides satisfying the optimality criterion, the scanning angle is confined by system constraints, such as the range of detection of the transducer or the physical dimensions of the tube/support structure. In this study the relationship between the scanning angle and the beam interactions at each boundary are given explicitly and analyzed to satisfy the optimality criterion.

The effect of refraction and reflection in the oblique angle scanning of a modified planar tube/support model is illustrated in Fig. 10. Mode conversion is evident at the liquid/solid interface, where the incident beam penetrates an elastic medium (solid) and creates two transmitted waves, one longitudinal and the other shear. The propagation of these two waves differ in intensity, direction, and velocity. However, liquid do not support the propagation of shear waves since they are inelastic by nature.

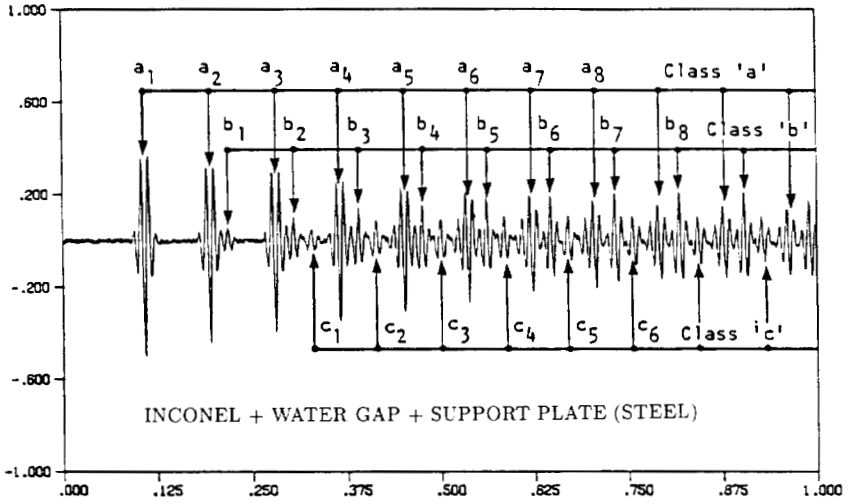

Fig. 8. Simulated results of backscattered signal from inspection of tube/support structure.

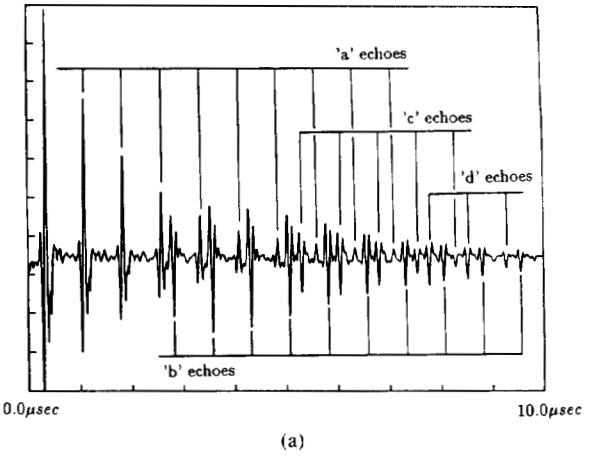

(a)

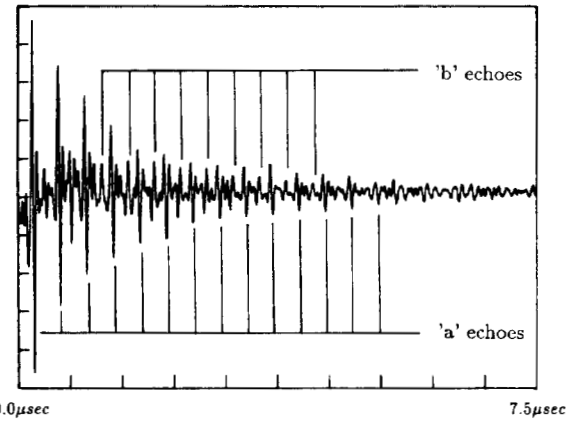

(b)

Fig. 9. Experimental results depicting reverberation process from A-scan of multilayered target consisting of four regions. (a) Planar model (water-aluminum-water-steel). (b) Tubular model (water-Inconel-water-steel).

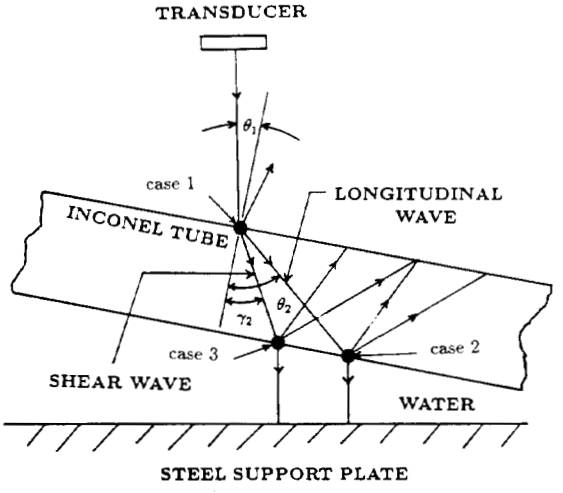

Fig. 10. Planar model of oblique angle scanning of tube/support structure.

The effect of the mode conversion at the solid interface increases the number of reverberant echoes tremendously.

The redirection of the incident energy is governed by Snell's Law:

$$\frac{\sin \theta_1}{v_{l1}} = \frac{\sin \theta_2}{v_{l2}} = \frac{\sin \gamma_2}{v_{s2}} \qquad (19)$$

where θ_i and γ_i are the angles (measured with respect to the normal of the boundary) and v_{li} and v_{si} are the velocities of the longitudinal and shear waves, respectively, in the given medium i (where medium 1 is liquid and medium 2 is solid). As can be seen from the preceding equation, the velocities of the waves before and after impinging the boundary determine the degree of refraction or reflection. The velocity of the longitudinal wave is approximately twice that of the shear wave in most materials, which infers that the longitudinal wave will have greater refraction than the shear wave for oblique angles.

The reflections and refractions that take place in the tube structure eliminate the detection of "a" echoes by directing the backscattered echoes away from the transducer. This can be seen in Fig. 11(a) (only the longitudinal class "a" echoes are shown for visual clarity). If the first reflected wave is out of the detection range, then all subsequent reverberations will not be detected, since the returning echoes are shifted laterally as the reverberations progress. The composite effect of this shifting will result in a greater rate of decay of the "a" echoes. It can be shown from (19) that as the scanning angle is in-

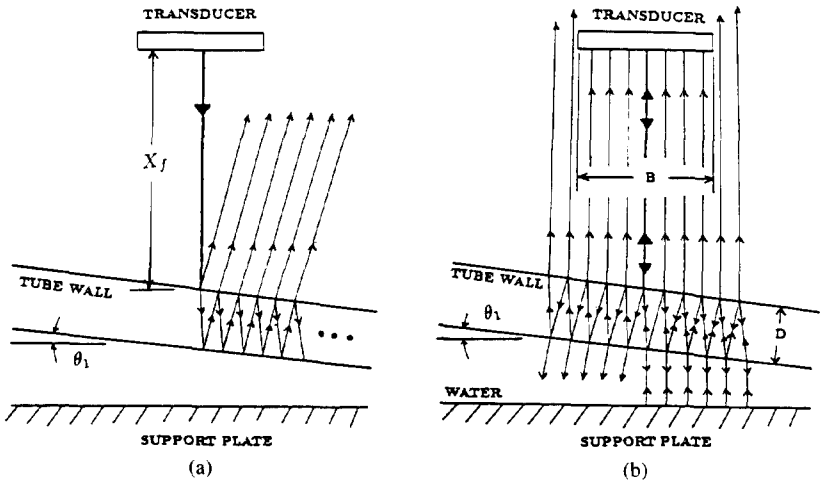

Fig. 11. (a) Progression of reverberations of "a" echoes. (b) Progression of "b" echoes in tube/support plate structure using OAS.

creased, the beams are reflected farther away from the transducer. Thus a lower bound on the scanning angle can be constructed to eliminate a significant amount of "a" echoes. This lower bound, $\theta_{1\min}$, can be derived from the geometry of Fig. 11(a):

$$\theta_{1\min} = \frac{1}{2}\tan^{-1}\left(\frac{B}{2X_f}\right) \tag{20}$$

where X_f is the path distance from the center of the transducer to tube wall and B is the beam field for class "a" rejection criteria. For example, the 20-MHz transducer used to obtain experimental data has a detection beam field of approximately 2 mm and a path distance, X_f, of 1.5 cm, which corresponds to a minimum angle of 1.9°.

Unlike the "a" echoes, the "b" echoes are preserved, since the angle of incidence of the returning echoes is equivalent to the initial incident beam. Fig. 11(b) illustrates the oblique angle scanning reverberation process for the "b" echoes, and to simplify the figure, does not show the shear waves or the "a" echo patterns. Although the returning "b" echoes have been unaltered in terms of direction in the refraction process, the "b" echoes have been shifted laterally, similar to the "a" echoes discussed previously. As the scanning angle increases, the refracted angles increase and lateral shifting becomes more dominant. Thus, to capture a minimum number of reverberations, an upper bound on the scanning angle, $\theta_{1\max}$, may be found by examining the geometry of Fig. 11(b), which gives

$$\cos\theta_1 = \frac{B}{DN\tan\theta_2} \tag{21}$$

where θ_1 is the incident angle, θ_2 is the longitudinal refracted angle, D is the tube thickness, N is the minimum number of returning echo paths detected, and B is the known beam field. Using Snell's law, (21) can be solved to find $\theta_{1\max}$:

$$\theta_{1\max} = \sin^{-1}\sqrt{\tfrac{1}{2}\left[(1+\eta^2) - \sqrt{(1+\eta^2)^2 - 4\eta^2k^2}\right]} \quad \text{for } k < 1 \tag{22}$$

where

$$k = \frac{v_{l1}}{v_{l2}} \quad \text{and} \quad \eta = \frac{B}{2ND}.$$

The preceding equation can be used to examine the number of possible "b" echoes that can be detected. For example, using a tube thickness of 1 mm and requiring five reverberations to be within the detection field forces an upper bound on the incident angle, $\theta_{1\max} = 2.7°$. In practice, the incident angle θ_1 must be bounded by $\theta_{1\min}$ and $\theta_{1\max}$, i.e.,

$$\theta_{1\min} \le \theta_1 \le \theta_{1\max}. \tag{23}$$

In general, the preceding condition may not be satisfied if the value of N exceeds the physical limits of the system. If this example is modified so that there are ten required reverberations, the result is $\theta_{1\max} = 1.4°$, which is contradictory to the optimal criterion. Equation (23) simplifies the analysis of the energy transfer functions of the reverberant tube/support plate structure considerably.

During the reverbation process of oblique angle scanning, there are three types of mode–boundary wave interactions that occur, which are circled in Fig. 10 and labeled "cases 1, 2, and 3." All three have different energy-transfer characteristics and contribute to the development of the "b" echoes in some way. The longitudinal wave incident on a liquid/solid boundary is referred to as case 1, as shown in Fig. 10. The case 1 interface determines how much of the energy that is transmitted into the tube wall. This energy must be maximized subject to the constraint given in (23). Case 2 corresponds to the situation of a longitudinal beam that is incident on a solid/liquid boundary in which its energy transfer characteristics describe how much energy leaks out of the tube wall and

also the degree of mode conversion. To increase the energy of the "b" echoes, transmission into the water gap should be maximized. Case 3 refers to a shear-wave incident on a solid/liquid boundary and has optimal requirements similar to case 2. The explicit solutions for the energy-transfer functions (i.e., shear and longitudinal) of these cases are known [6], [10], assuming that the incident beam is a plane harmonic wave and that the boundary is homogeneous.

Wave generation for case 1 consists of one reflected wave and two transmitted waves in which the energy relationships with respect to the incident beam are given [6], [10] as

$$\left(\frac{\varphi_1'}{\varphi_1}\right)^2 = \left|\frac{-Z_1 G_{l2} G_{s2} + G_{s2}\cos^2 2\gamma_2 + G_{l2}\sin^2 2\gamma_2}{Z_1 G_{l2} G_{s2} + G_{s2}\cos^2 2\gamma_2 + G_{l2}\sin^2 2\gamma_2}\right|^2 \tag{24}$$

$$\left(\frac{\varphi_2}{\varphi_1}\right)^2 = \frac{4\rho_1 \tan\theta_1}{\rho_2 \tan\theta_2} \cdot \left|\frac{G_{s2}\cos 2\gamma_2}{Z_1 G_{l2} G_{s2} + G_{s2}\cos^2 2\gamma_2 + G_{l2}\sin^2 2\gamma_2}\right|^2 \tag{25}$$

$$\left(\frac{\psi_2}{\varphi_1}\right)^2 = \frac{4\rho_1 \tan\theta_1}{\rho_2 \tan\gamma_2} \cdot \left|\frac{G_{l2}\sin 2\gamma_1}{Z_1 G_{l2} G_{s2} + G_{s2}\cos^2 2\gamma_2 + G_{l2}\sin^2 2\gamma_2}\right|^2 \tag{26}$$

where subscript 1 indicates the propagating medium is water, and subscript 2 indicates the propagating medium is Inconel (hardened steel). The variables used in all three cases represent

- φ_i intensity of the longitudinal wave in region i,
- φ_i' intensity of the reflected longitudinal wave in region i,
- ψ_i intensity of the shear wave in region i,
- ψ_i' intensity of the reflected shear wave in region i,
- θ_i angle of the longitudinal wave in region i,
- γ_i angle of the shear wave in region i,
- ρ_i density of the region i,
- v_{li} velocity of the longitudinal wave in region i,
- v_{si} velocity of the shear wave in region i.

Also, in order to simplify the energy relationships, the acoustic impedance and admittance will be defined as

$$Z_1 = \frac{\rho_1 v_{l1}}{\cos\theta_1} \quad Z_{l2} = \frac{\rho_2 v_{l2}}{\cos\theta_2} \quad Z_{s2} = \frac{\rho_2 v_{s2}}{\cos\gamma_2} \tag{27}$$

$$G_{l2} = \frac{1}{Z_{l2}} \quad G_{s2} = \frac{1}{Z_{s2}} \tag{28}$$

where subscripts l and s refer to the longitudinal and shear waves, respectively. The energy conversion characteristics of the reflected and refracted waves are examined using computer simulation, and the value of the parameters used in this simulation are

$$\rho_1 = 1.00\ (\text{g/cm}^3) \quad v_{l1} = 1.483\ (\text{km/s})$$
$$v_{s1} = 0.000\ (\text{km/s})$$
$$\rho_2 = 8.51\ (\text{g/cm}^3) \quad v_{l2} = 5.476\ (\text{km/s})$$
$$v_{s2} = 3.302\ (\text{km/s}).$$

The intensity of the normalized waves versus the incident angle θ_1, are shown in Fig. 12. In keeping with the previous constraints of θ_1 being less than approximately three degrees, the amount of energy transmitted into the medium is relatively constant in this interval. This can be assessed by observing the reflected energy, $(\varphi_1'/\varphi_1)^2$, in this interval. As can be seen from Figs. 12(c) and 12(d), changing the incident angle would only transfer the energy from one mode to the other. It is important to point out that the amount of transmitted shear wave is significantly smaller than the longitudinal wave over the angles of interest.

The energy relationships between the transmitted and reflected waves with respect to the incident beam for case 2 are as follows [6], [10]:

$$\left(\frac{\varphi_2'}{\varphi_2}\right)^2 = \left|\frac{Z_1 G_{l2} G_{s2} - G_{s2}\cos^2 2\gamma_2 + G_{l2}\sin^2 2\gamma_2}{Z_1 G_{l2} G_{s2} + G_{s2}\cos^2 2\gamma_2 + G_{l2}\sin^2 2\gamma_2}\right|^2 \tag{29}$$

$$\left(\frac{\varphi_1}{\varphi_2}\right)^2 = \frac{Z_1 G_{l2}}{\cos^4 2\gamma_2}\left|1 - \frac{\varphi_2'}{\varphi_2}\right|^2 \tag{30}$$

$$\left(\frac{\psi_2'}{\varphi_2}\right)^2 = \left(\frac{v_{s2}}{v_{l2}}\right)^4 \frac{\tan\theta_2 \sin^2 2\theta_2}{\tan\gamma_2 \cos^2 2\gamma_2}\left|1 - \frac{\varphi_2'}{\varphi_2}\right|^2. \tag{31}$$

The plot of the intensity of normalized waves against the range of incident angles θ_1 is shown in Fig. 13. Fig. 13(b) reveals that in the transmitted energy $(\varphi_1/\varphi_2)^2$ maximization occurs when the scanning angle is minimized. This minimization also results in making the longitudinal waves more dominant, and mode conversion becomes negligible at this interface.

The energy relationship between the transmitted and reflected waves and the incident wave for case 3 are [6], [10]

$$\left(\frac{\psi_2'}{\psi_2}\right)^2 = \left|\frac{Z_1 G_{l2} G_{s2} + G_{s2}\cos^2 2\gamma_2 - G_{l2}\sin^2 2\gamma_2}{Z_1 G_{l2} G_{s2} + G_{s2}\cos^2 2\gamma_2 + G_{l2}\sin^2 2\gamma_2}\right|^2 \tag{32}$$

$$\left(\frac{\varphi_2'}{\psi_2}\right)^2 = \left(\frac{v_{l2}}{v_{s2}}\right)^4 \frac{\tan\gamma_2 \cos^2 2\gamma_2}{\tan\theta_2 \sin^2 2\theta_2}\left|1 - \frac{\psi_2'}{\psi_2}\right|^2 \tag{33}$$

$$\left(\frac{\varphi_1}{\psi_2}\right)^2 = \frac{\rho_1 \tanh\theta_1}{2\rho_2 \sin 2\gamma_2 \sin^2\gamma_2}\left|1 - \frac{\psi_2'}{\psi_2}\right|^2. \tag{34}$$

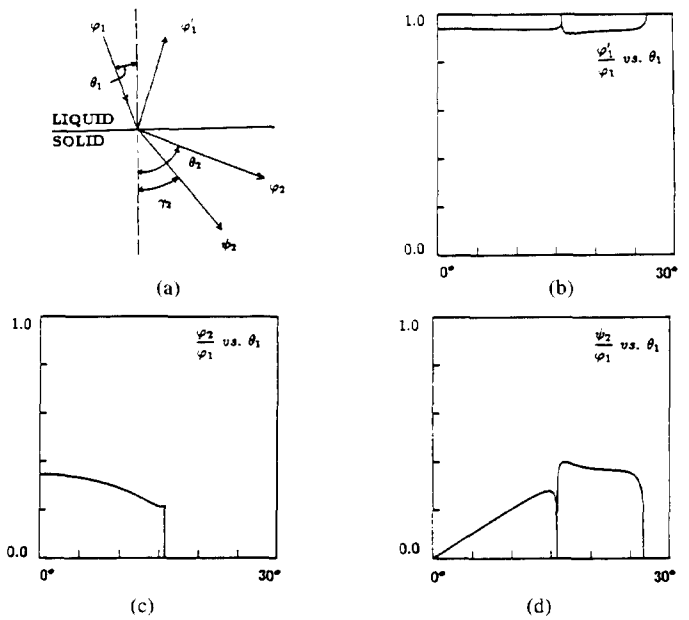

Fig. 12. (a) Geometrical representation of refracted and reflected waves for case 1. (b)–(d) Respective intensities of refracted (φ_2, ψ_2) and reflected (φ_1') waves as function of θ_1.

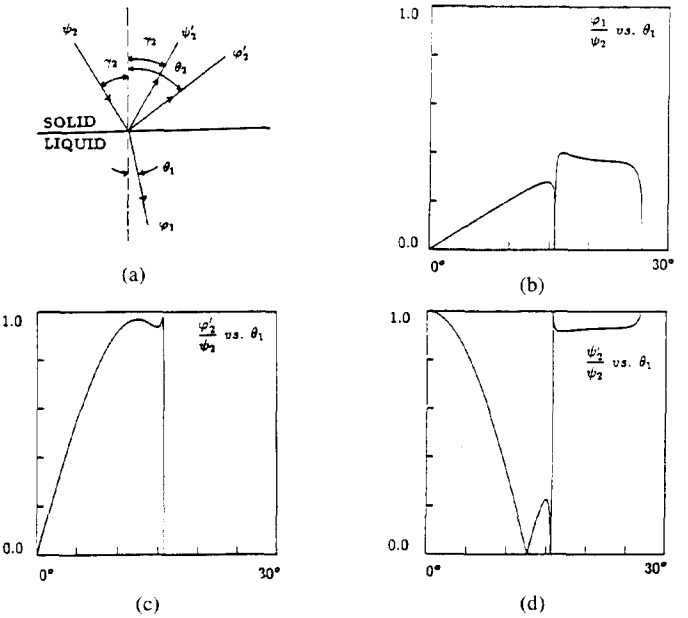

Fig. 14. (a) Geometrical representation of refracted and reflected waves for case 3. (b)–(d) Intensities of refracted (φ_1) and reflected (φ_2', ψ_2') waves as function of θ_1.

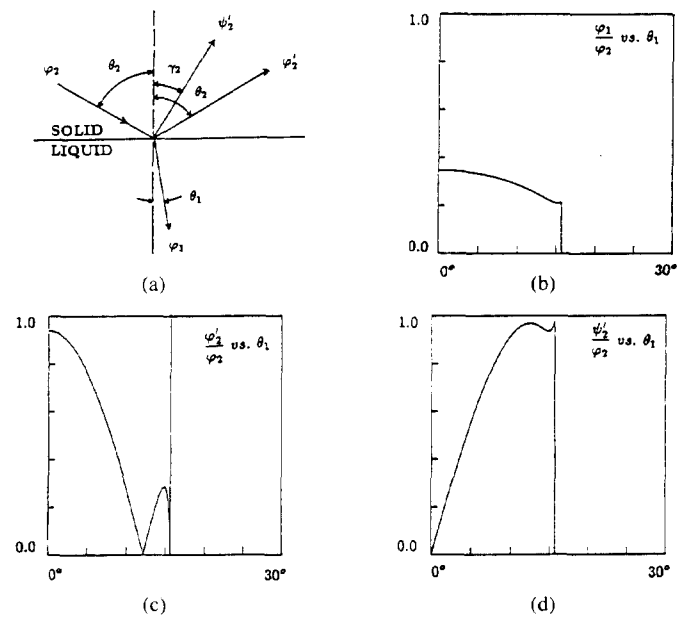

Fig. 13. (a) Geometrical representation of refracted and reflected waves for case 2. (b)–(d) Intensities of refracted (φ_1) and reflected (φ_2', φ') waves as function of θ_1.

The preceding energy relationships versus the incident angle θ_1 can be seen in Fig. 14. Fig. 14(b) indicates that the transmitted energy, $(\varphi_1/\psi_2)^2$, into the water gap will increase by increasing the incident angle. This will also result in increasing mode conversion and the generation of surface waves.

In consolidating the results of the three previous paragraphs, it becomes apparent that minimization of the shear waves and mode conversion would be concurrent with the optimality criteria. This is supported by the fact that cases 1 and 2 are not efficient in producing shear waves. Furthermore, in comparing cases 2 and 3, as far as effectiveness in transmitting energy into the water gap, case 2 transmits considerably more energy. Thus the smallest scanning angle should be chosen in order to minimize the energy lost in mode conversion and to maximize the intensity of the "b" echoes.

OAS Experimental Patterns

Oblique angle measurements were made using planar and tubular multilayered models. Within the permissable range of scanning angles given in (23), experimental results have been found to be concurrent with theoretical predictions. Planar measurements were taken using several angles inside and outside the bounds described by (23), showing how the characteristics of "b" echoes are affected as a function of the incident angle. Similar results were observed using the tubular model. Both planar and tubular measurements demonstrated the effectiveness of OAS in recovering information from the target hidden by a highly reverberant thin layer.

The setup for the planar OAS measurements is similar to that shown in Fig. 10. The front-layer thickness is 2 mm, a target distance of 5 cm, and the 3-dB beam field of the transducer used is approximately 6 mm. The constraints on the incident angle are $1.74° \leq \theta_1 \leq 4.15°$, where at least five reverberations are within the 3-dB beam field. The three measurements are shown in Fig. 15, where the scanning angles are 0.35°, 1.94°, and 5.10°. In Fig. 15(a), class "a" echoes are interfering with "b" echoes, which makes direct evaluation difficult. As the angle is increased to 1.94° (shown in Fig. 15(b)), "a" echoes are completely eliminated from the region of interest. The

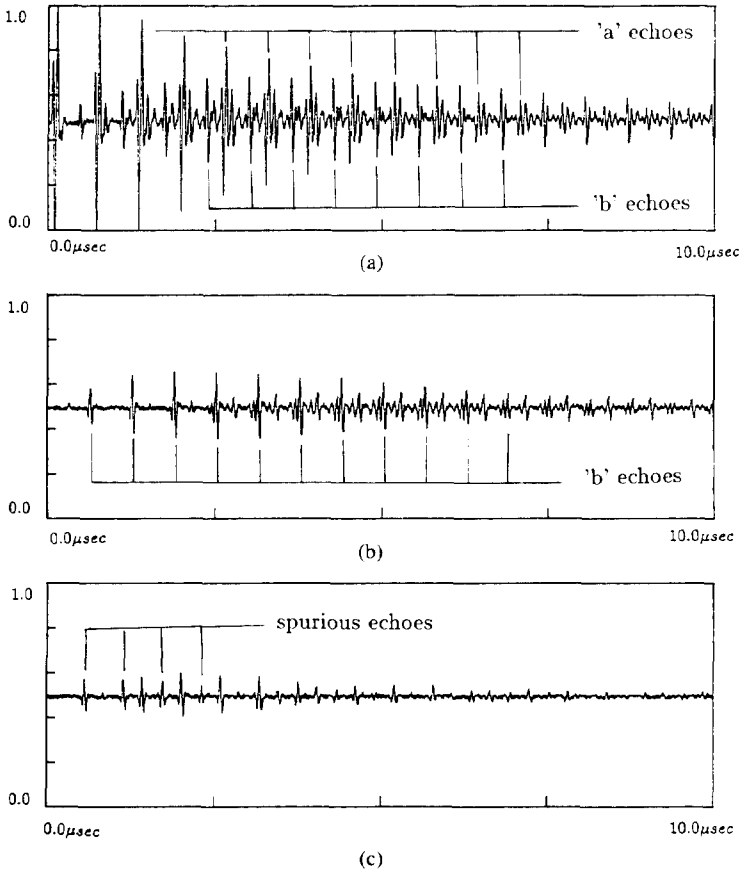

Fig. 15. OAS experimental results from planar model. (a) $\theta_1 = 0.35°$. (b) $\theta_1 = 1.94°$. (c) $\theta_1 = 5.1°$.

"b" echoes are clearly visible, bearing minimal distortion. However, if the angle is increased further to 5.1°, then the "b" echoes decrease in magnitude, as shown in Fig. 15(c), due to the lateral shifting of the echoes out of the detectable field of the transducer, as discussed earlier. In addition, echoes not accounted for in the model are present due to the effect of mode conversion.

The tubular measurements using OAS are shown in Fig. 16. These measurements follow the constraints calculated in the theoretical analysis, in which the scanning angle used was approximately two degrees. Fig. 16(a) shows the results of the OAS of the tube structure without the support plate behind it, displaying only "a" echoes. The rejection of "a" echoes is evident, although more noise is observed because the measurements are taken in an enclosed space and all the reverberant echoes are trapped within the structure. Fig. 16(b) shows the OAS of the tube/support plate, in which the "b" echoes are clearly visible and resolvable. These results can be beneficial in characterizing the support plate integrity. It is important to mention that the oblique angle scanning scheme performs well for the case where the target is orientated in such a manner to reflect a sufficient amount of energy towards the transducer [12]. In general, OAS can be employed in examining multilayered structures where cracks or flaws are present and where normal incident scanning proves ineffective.

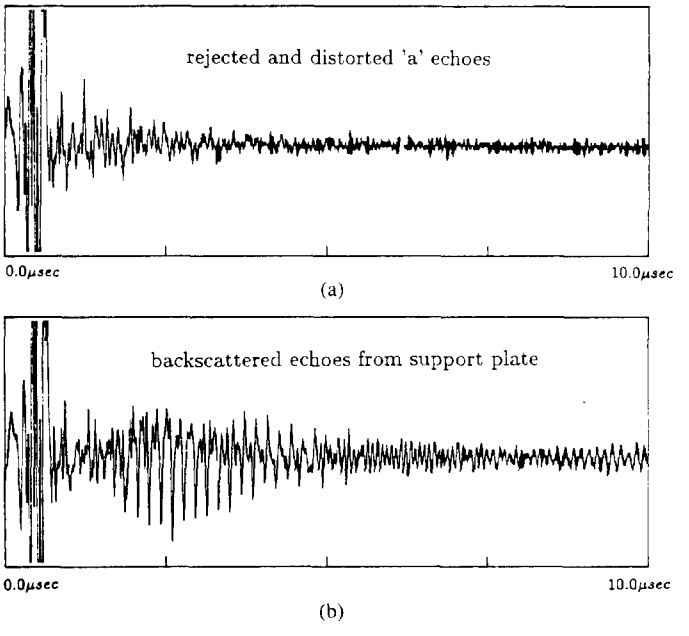

Fig. 16. OAS experimental results from tubular models. (a) A-scan of tube wall. (b) A-scan tube wall with support plate behind it.

Patterns Associated with Deteriorated Layers

The ultrasonic evaluation of the integrity of tube/support structures in the presence of inhomogeneuities (i.e., corrosion and/or flaws) becomes very difficult and re-

quires a high-performance measuring system. For all data acquisitions presented in this section, a 20-MHz focused transducer with a 3-dB bandwidth of 10 MHz was used, which provided resolution of about 20 μm in water. The resolution of the transducer cannot be improved without increasing the frequency, but in doing so, the energy of the backscattered signal will decrease significantly due to absorption and scattering caused by the granular characteristics of the material. Another important feature of this transducer is its focusing capabilities, since the tubular geometry of the target is a source of distortion as the traveling time of the echoes varies with position. Proper focusing decreases the spreading of the incident beam and consequently limits the amount of distortion introduced to the signal. Thus the resolution, focusing characteristics, and sensitivity of the transducer do play a significant role in its performance.

Several measurements were taken to display predictable experimental results corresponding to different deterioration scenarios of the tube/support structure. These scenarios are concerned with the detection of flaws within the tube wall or corrosion growth stemming from the support plate. This structural deterioration will cause a reduction in the energy of the back-scattered signal, although the effects on the class "a" and class "b" echoes differ with scenario.

The deterioration of the tube wall in terms of flaws and erosion results in significant attenuation of the "a" echoes caused by scattering. To illustrate the effect flaws have on the reverberant patterns, two tube samples have been altered by drilling a tapered notch in depths of 100 and 200 μm. The resulting back-scattered signals can be seen in Fig. 17, where the signal intensity suffers and, as expected, is dependent on the size of the notch. For the tube containing a 100-μm notch, the back-scattered signal is shown in Fig. 17(b), the signal intensity drops 6 dB compared to the reference signal shown in Fig. 17(a), and in Fig. 17(c) the 200-μm notch causes the signal to decay an additional 3 dB. This confirms the reliability of examining "a" echoes to evaluate the overall condition of the tube wall in which inhomogenuities of relatively small size can be characterized. Thus the evaluation of the tube wall can be obtained from a mapping of these patterns, which provide information of location and depth of the dents or flaws.

To simulate the effects of tube erosion, the surface of a sample has been tapered as shown in Fig. 18(a). The smallest thickness of the tapered tube is 37.5 mil, which might be greater than would occur in general, but is done to emphasize its effect on the received signal. Results of the radial scanning of the tapered tube can be seen in Fig. 18(b), containing nine measurements, referred to as traces 1–9. In comparison to trace 1 (the reference signal), trace 2 reveals rejection of the signal similar to that seen in the oblique angle analysis, where a majority of the backscattered signal is directed out of the detection field of the transducer. This creates another practical application of

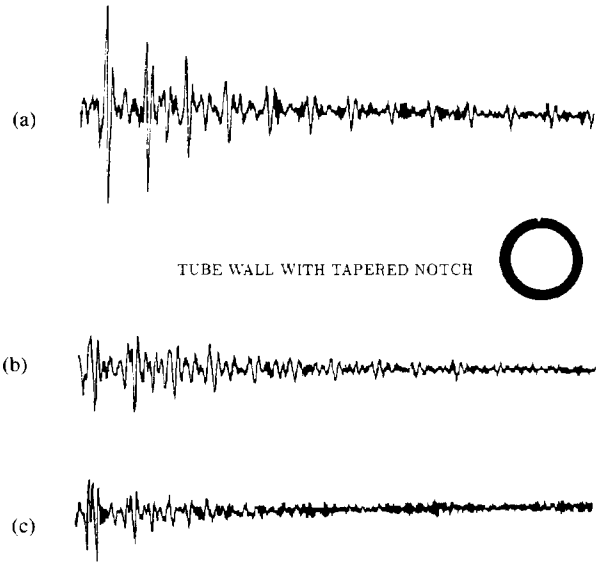

Fig. 17. Reverberant patterns derived from tube samples with tapered dents. (a) Depth of taper is zero for reference signal. (b) Depth of taper is 100 μm for reference signal. (c) Depth of taper is 200 μm for reference signal.

OAS in which the search for reflectors oriented at some angle can describe the degree of erosion present. Traces 3–5 show progressive improvements in the received signal, since the outer surface of the tube wall becomes more parallel to the inner wall and thus a greater amount of energy is directed back towards the transducer. The reproducibility of these measurements can be seen in traces 6–9, where few variations are discernable from the geometry of the opposing traces. Also, as the tube-wall thickness reduces, the distance between "a" echoes decreases, which is evident when comparing traces 1 and 5.

In examining the corrosion growth stemming from the support plate, several deteriorated samples were examined which illustrate common patterns associated with different degrees of corrosion. The first sample corresponds to the case where corrosion is significant but has not completely filled the water gap between the tube wall and support plate. The radial scan of the first sample can be seen in Figs. 19(a)–(c), where each trace was taken at different positions. In the traces of Figs. 19(a)–(c), the presence of "b" echoes is practically nonexistent. This is expected due to the poor reflective properties of the support plate resulting from the presence of corrosion. Also, Fig. 19(b) displays signs of disruption in the tube wall since the "a" echoes are less reverberant than in the other traces. This effect can be seen more clearly in latter reverberations of the "a" echoes. Thus observations of later reverberations will be conducive for detecting significant deterioration in the "a" and "b" echoes due to corrosion growth.

In cases where severe corrosion growth effects the tube wall, several patterns can be anticipated. A high degree of corrosion alters the tube wall upon contact, which scatters and distorts both the "a" and "b" echoes. The traces Figs. 19(d) and 19(e) show the radial scan of a corroded

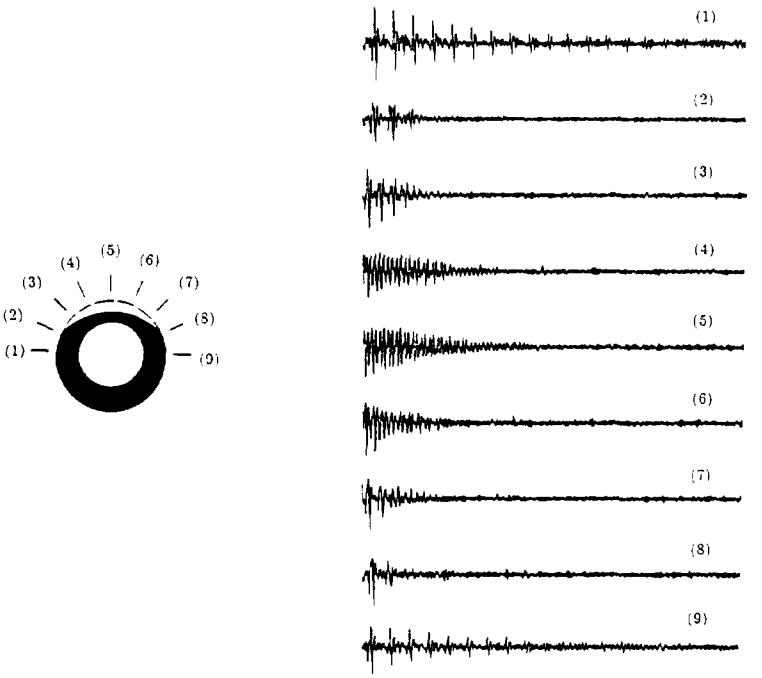

Fig. 18. Tube erosion study. (a) Schematic of altered tube. (b) Traces 1–9 are radial scanned measurements of erroded tube.

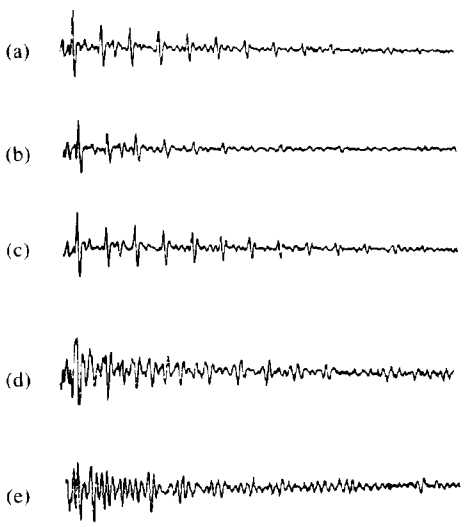

Fig. 19. A-scan of corroded tube/support structure. (a)–(e) Various measurements shown in traces.

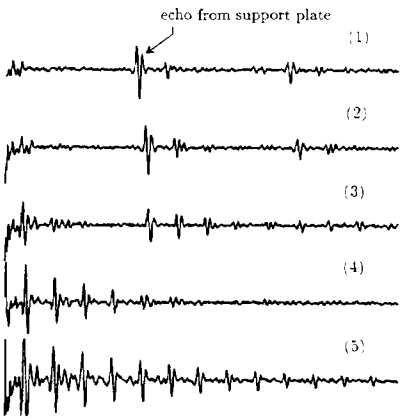

Fig. 20. Reverberant patterns showing different scenarios that may be present in case of severe corrosion.

and dented sample in which scattering effects are apparent in reverberation patterns. Slight resemblance to tube echoes can be seen from these figures, although the patterns are very sporadic and random in nature. Another possible effect of severe corrosion is displayed in Fig. 20, where large pulses appear after some delay, not corresponding to the expected reverberant patterns. This is a direct result of the corrosion diffusing into the tube wall. This alters the previous multilayered structure because that reverberation exists mainly between the inner surface of the tube wall and the support plate. However, in traces 3–5 it can be seen that diffusion is not complete and reverberations will exist within the tube wall as well. This diffusion provides another scenario that must be taken into account in characterizing the tube/support structure.

Conclusion

It has been demonstrated that the concept of echo classification is essential in the ultrasonic evaluation of reverberant multilayered targets. This provides methods of correlating patterns of the back-scattered signal with the integrity of different layers of the multilayered structure. The alternative OAS method can further enhance the performance of this classification scheme, which has the capability of rejecting front-layer back-scattered echoes while preserving the information-bearing echoes from the

target behind the reverberant layer. The improvement in visibility of the "b" echoes is very significant, as presented in experimental measurements, and this allows for direct evaluation of hidden targets. In general, the visibility of "a" and "b" echoes is not guaranteed, and further processing is warranted (e.g., echo cancellation and spectral analysis [11]). It has been shown that patterns associated with corrosion for several frequently occuring cases are recognizable, although to produce guidelines for the characterization of complex patterns, a large spectrum of samples is needed to determine their growth and corresponding reflective properties.

References

[1] H. H. Chaakelis and A. V. Clark, "Ultrasonic nondestructive bond evaluation: An analysis of the problem," *Materials Eval.*, vol. 38, pp. 20-38, 1980.

[2] J. Krautkramer, *Ultrasonic Testing of Materials*. New York: Springer-Verlag, 1975.

[3] S. Lees, "Ultrasonic measurement of thin layers," *IEEE Trans. Sonics Ultrason.*, vol. SU-18, no. 2, pp. 81-88, 1971.

[4] J. L. Rose and P. A. Meyer, "Ultrasonic signal processing concepts for measuring the thickness of thin layers," *Materials Eval.*, vol. 32, pp. 249-255, 1974.

[5] G. Maze, J. L. Izbicki, J. Ripoche, A. Nagl, H. Uberall, and K. B. Yoo, "Transient acoustic scattering from layers and plates," *J. Acoust. Soc. Am.*, vol. 80, pp. 295-301, 1986.

[6] L. M. Brekhovskikh, *Waves in Layered Media*, T. Beyer, Translat. and Ed. New York: Academic, 1980.

[7] J. Saniie, E. S. Furgason, and V. L. Newhouse, "Ultrasonic imaging through highly reverberant thin layers—Theoretical considerations," *Materials Eval.*, vol. 40, pp. 115-121, 1982.

[8] J. Saniie, "Ultrasonic signal processing: System identification and parameter estimation of reverberant and inhomogeneous targets," Ph.D. thesis, Purdue Univ., 1981.

[9] J. Saniie and D. T. Nagle, "On the imaging of tube/support structure of power plant steam generators," in *Review of Progress in Quantitative NDE*, Vol. 6a, D. O. Thompson and D. E. Chimenti, Eds. New York: Plemnum, 1987, pp. 519-525.

[10] W. M. Ewing, W. S. Jardetzky, and F. Press, *Elastic Waves in Layered Media*. New York: McGraw-Hill, 1957.

[11] J. Saniie, "Resolution and visibility enhancement of ultrasonic echoes reflected from targets hidden by highly reverberant layers," *IEEE Ultrason. Proc.*, Dallas, TX, 1984, pp. 903-907.

[12] D. S. Kupperman, M. J. Caines, and A. Winieki, "Assessment of ultrasonic NDE methods for ceramic heat-exchanger tubes," *Mat. Eval.*, vol. 40, pp. 774-782, 1982.

Jafar Saniie (S'80-M'81) was born in Iran in March of 1952. He received the B.S. degree in electrical engineering from the University of Maryland in 1974. In 1977 he received the M.S. degree in biomedical engineering from Case Western Reserve University, and in 1981, the Ph.D. degree in electrical engineering from Purdue University.

In 1981 he joined the Applied Physics Laboratory, University of Helsinki, Finland, to conduct research in photothermal and photoacoustic imaging. Since 1983 he has been with the Department of Electrical and Computer Engineering, Illinois Institute of Technology, where he is an Associate Professor and Director of the Ultrasonic Information Processing Laboratory. His current research activities include radar signal processing, estimation and detection, computer and tomography, and ultrasonic imaging with both industrial and biomedical applications.

Dr. Saniie is member of the IEEE, Tau Beta Pi, Eta Kappa Nu, and has been an IEEE Student Branch Counselor since 1983. He is the 1986 recipient of the Outstanding IEEE Student Counselor Award.

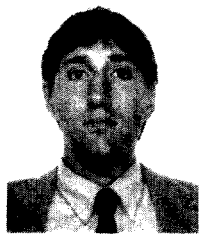

Daniel T. Nagle (S'85-M'85-S'86-M'86-S'87) was born in Chicago, IL, on April 22, 1963. He received the B.S. and M.S. degree in electrical engineering from the Illinois Institute of Technology in 1985 and 1987, respectively. He is currently pursuing the Ph.D. degree in the area of digital signal processing and communication systems.

His research entails statistical pattern recognition, ultrasonic signal, and image processing.

Mr. Nagle is a member of Eta Kappa Nu and Phi Kappa Sigma.